Degenerate four-wave mixing and photofragment yield spectroscopic study of jet-cooled SO_2 in the $\tilde{C}\ ^1B_2$ state: Internal conversion followed by dissociation in the $\tilde{X}$ state

Akihiro Okazaki, Takayuki Ebata, and Naohiko Mikami
Department of Chemistry, Graduate School of Science, Tohoku University, Sendai 980-77, Japan

(Received 12 August 1997; accepted 27 August 1997)

The predissociation mechanism of the $\tilde{C}$ state of SO_2 have been investigated by the measurements of degenerate four-wave mixing (DFWM), laser-induced fluorescence (LIF) and photofragment yield spectra. The DFWM spectrum of jet-cooled SO_2 was measured under a high power condition where the DFWM signal corresponds well to the absorption spectrum. Relative fluorescence quantum yields of various vibronic bands were obtained by comparing the DFWM spectrum with the LIF spectrum. It was found that the fluorescence quantum yields of the vibronic levels involving anti-symmetric stretching (ν_3) vibration are considerably smaller than those of other levels. The result indicates that the nonradiative process of the $\tilde{C}$ state is initiated as the internal conversion to the $\tilde{X}$ state and ν_3 acts as the promoting mode. By observing the O atom photofragment yield spectrum we confirmed that the predissociation occurs from the (1,4,2) level. Vibronic dependence of the rise time of the O atom generation was found to be in accordance with those of the fluorescence decay rate. The obtained results represent that the dissociation occurs immediately after the internal conversion to the $\tilde{X}$ state. © *1997 American Institute of Physics.* [S0021-9606(97)02145-4]

I. INTRODUCTION

From a viewpoint of photochemical importance, the $\tilde{C}$ state of SO_2 have been extensively studied for many years with various spectroscopic methods.[1–14] Okabe first found a sudden decrease of the fluorescence intensity in the $\tilde{C}\ ^1B_2 \leftarrow \tilde{X}\ ^1A_1$ transition starting from 240 nm and showed that the predissociation threshold lies at $\approx$219 nm.[1] Hui *et al.* measured the fluorescence lifetimes of the $\tilde{C}$ state and found that the lifetime of $\approx$45 ns at 221 nm decreases to $\approx$8 ns at 215 nm.[2] Ivanco *et al.* observed quantum beats in the fluorescence decay from the $\tilde{C}$ state. They argued that the quantum beats disappear at the onset of predissociation ($\approx$218 nm) and suggested that the predissociation is due to the vibronic coupling between the $\tilde{C}$ state and $\tilde{X}$ state.[3] On the other hand, Kanamori *et al.* observed inverted population distribution of triplet sublevels of the SO ($X\ ^3\Sigma^-$) fragment by infrared (IR) absorption spectroscopy, suggesting a decay channel to a triplet state.[4] Ebata *et al.*, observed the LIF spectrum of jet-cooled SO_2 and reported the predissociation threshold at 45 400 cm^{-1} ($\approx$220 nm) and that the dissociation rates depend on rovibronic levels.[5] The rotational level dependence of the predissociation rate has been presented by Becker *et al.* who identified that the predissociation occurs above $J'=5$ of the $\tilde{C}$ (1,4,2) band.[6,7] In spite of extensive works, there has not been the conclusive evidence reported whether the predissociation occurs through singlet or triplet surface. One of the reasons is due to the difficulty in obtaining fluorescence quantum yield (FQY) in a supersonically cooled condition. In particular, it is necessary to observe the absorption spectrum for jet-cooled SO_2 to obtain FQY.

In the present work, we applied several spectroscopic methods to investigate the predissociation mechanism of the $\tilde{C}$ state. We observed (1) degenerate four-wave mixing (DFWM) spectrum, (2) LIF spectrum, and (3) photofragment yield spectrum for the $\tilde{C} \leftarrow \tilde{X}$ transition of jet-cooled SO_2. We observed the DFWM spectrum at higher laser power limit where the signal intensity is proportional to the absorption cross section. By comparison between the DFWM and LIF intensities, the relative fluorescence quantum yield (RFQY) was obtained. We also measured fluorescence lifetimes of the vibronic levels of the $\tilde{C}$ state. From the results of the RFQY and lifetime measurements, we found that the logarithmic plot of the decay rate linearly increases with the energy and that the vibronic levels involving anti-symmetric vibration (ν_3) have larger nonradiative decay rate than other levels. The photofragment yield spectrum of O atom generation and its rise time were observed by pump–probe method. By comparison between the photofragment yield and LIF spectra we confirmed that the dissociation occurs from the (1,4,2) level of the $\tilde{C}$ state. The production rate of O atom fragment showed good correlation with the fluorescence decay rate. The predissociation mechanism of the $\tilde{C}$ state SO_2 is discussed based on the results.

II. EXPERIMENT

A schematic diagram of the experimental setup for the DFWM spectroscopy is shown in Fig. 1. A frequency doubled output of an excimer laser pumped dye laser (Lambda Physik EMG103MSC/FL2002E) was split into three beams with equal intensity. The intensity of each beam was typically 40 μJ and the resolution was 0.2 cm^{-1}. The three beams were directed into a vacuum chamber in the forward geometry similar to that reported by Butenhoff *et al.*[15,16] The three beams crossed at 10–15 mm downstream

 0021-9606/97/107(21)/8752/7/$10.00

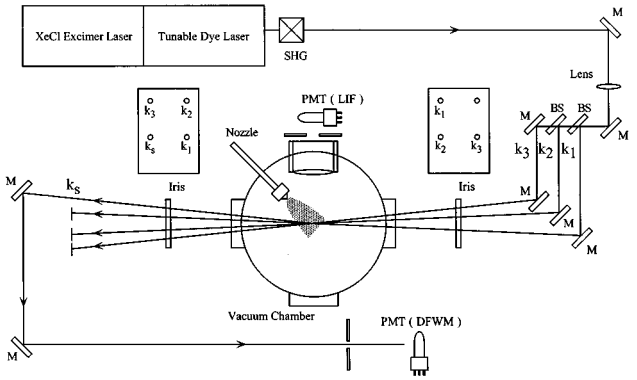

FIG. 1. Experimental setup of DFWM spectroscopy. The abbreviations used in the figure are defined as follows: M, mirror; BS, beamsplitter; PMT, photomultiplier tube.

of a pulsed nozzle having an orifice of 400 μm. The DFWM signal beam was detected by a photomultiplier tube (PMT) (Hamamatsu Photonics 1P28) located at 2 m apart from the chamber. The LIF was detected perpendicularly to both molecular and laser beams by an another PMT. These signals were averaged by a boxcar integrator (PAR Model 4420) connected with a computer. Fluorescence lifetime measurements were done by using a 500 MHz digital oscilloscope (Sony Tektronics TDS 520). By use of the time profile of the scattering laser pulse which was monitored by PMT, the fluorescence lifetime of each vibronic level was obtained by fitting the convoluted decay curve.

Since the predissociation from the $\tilde{C}$ state of SO_2 leads to SO ($X\ ^3\Sigma^-$) and O (^3P_j) fragments, the generation of the latter can be investigated by using a $(2+1)$ REMPI through the $^3P_{j'} \leftarrow {}^3P_{j''}$ transition at 226 nm.[7] The second harmonics of a dye laser, which is referred to a probe laser, was used to detect the O atom. A frequency doubled output of an Nd:YAG laser pumped dye laser (Continuum Powerlite 9010/Lumonics HD500) was used for the excitation of SO_2 molecule, and a second harmonics of excimer laser pumped dye laser (Lambda Physik LEXTRA 50/Scanmate 2E) was used for the probe of the fragment. Both light beams were introduced into the chamber with a counterpropagated geometry. The ions generated by REMPI were separated by a time-of-flight (TOF) tube and were detected by an electron multiplier (Murata Ceratron). The ion signal was amplified and integrated by the boxcar integrator (PAR Model 4420). The typical delay time between the dissociation and probe lasers for the observation of the photofragment was set to 20 ns, which was accurately provided by using a delay generator (SRS Model DG535). The production rates of the O atom fragment were obtained by changing the delay time between the dissociation and the probe lasers.

III. RESULTS AND DISCUSSION

A. Measurement of relative fluorescence quantum yield (RFQY) of the $\tilde{C}$ state

The expression of the DFWM intensity with respect to collisional, polarization, and saturation effects has been presented by many theoretical studies.[17–32] The simplest analytical model for DFWM of two level system was reported by Abrams and Lind (AL),[18,19] and has been shown a good agreement with the experiments.[17,33] According to AL model, the DFWM intensity, I_s, is given by

$$I_s \approx (\alpha_0 L)^2 \frac{1}{1+\delta^2} \frac{4I^3/I_{\rm sat}^2}{(1+4I/I_{\rm sat})^3}, \tag{1}$$

$$\alpha_0 = \frac{\omega_{ge} T_2}{2c\hbar\epsilon_0} |\mu_{ge}|^2 \Delta N_0. \tag{2}$$

In this expression, I refers to the input laser power, μ_{ge} to the transition dipole moment connecting between lower (g) and upper (e) levels, L to the interaction length of three laser beams, $\delta = (\omega - \omega_{ge}) T_2$ to the detuning of the probe (ω) and transition (ω_{ge}) frequencies and ΔN_0 is the population difference between the ground and excited states. $I_{\rm sat}$ is called line-center saturation intensity, which is defined by

$$I_{\rm sat} = \frac{c\hbar^2 \epsilon_0}{2T_1 T_2 |\mu_{ge}|^2}, \tag{3}$$

where T_1 and T_2 represent the population and the coherence decay time, respectively. The dependence of the DFWM signal amplitude on the intensities of input laser beams can be expressed by assuming the limiting forms of Eq. (1); for $I \gg I_{\rm sat}$

$$I_s \propto \alpha_0^2 L^2 I_{\rm sat} \propto |\mu_{ge}|^2 T_1^{-1} T_2 I_{\rm total}^0, \tag{4}$$

and for $I \ll I_{\rm sat}$

$$I_s \propto \alpha_0^2 L^2 4I^3/I_{\rm sat}^2 \propto |\mu_{ge}|^8 T_1^2 T_2^4 I_{\rm total}^3. \tag{5}$$

T_1 and T_2 are related to the collisional dephasing rate γ_c by[32]

$$\frac{1}{T_2} = \frac{1}{2T_1} + \gamma_c. \tag{6}$$

Since $2T_1 = T_2$ for collision-free environment in a supersonic molecular beam, the DFWM spectrum obtained under the condition of $I \gg I_{\rm sat}$ turns out to be proportional to $\sigma = |\mu_{ge}|^2$, which is similar to the absorption spectrum.

To investigate the relationship between $I_{\rm sat}$ and σ for the $\tilde{C} \leftarrow \tilde{X}$ transition of SO_2, the measurement of the power dependence of the DFWM intensity was done for the prominent vibronic bands of the $\tilde{C}$ state. Figure 2 shows the results of the power dependence of the DFWM signal for the (1,5,2) band. Also shown is the simulated curve fitted by using Eq. (1). As seen in Fig. 2, the observed power dependence is fitted very well with the simulated power dependence by using Eq. (1). Williams *et al.* has measured the DFWM spectrum of CH radical and reported the laser power dependence of the DFWM line-center intensity.[21,33] They showed that the observed DFWM intensity of the CH radical was in good agreement with that predicted by Eq. (1) and that the DFWM intensity was saturated at higher power region. Thus, we can use Eq. (4), which is the high power limit of Eq. (1) and the relative peak intensity at the saturated condition is proportional to the absorption cross section. The laser power was

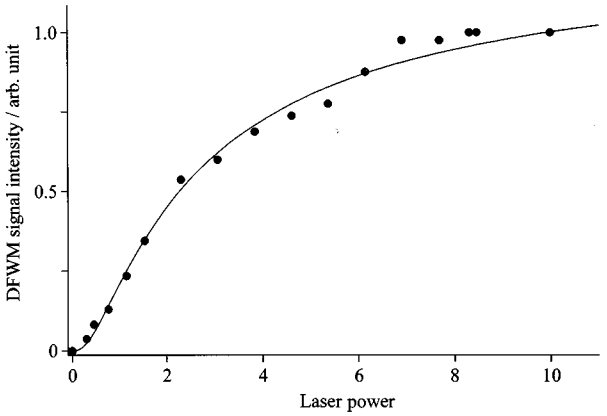

FIG. 2. Laser power dependence of the DFWM signal of (1,5,2) band. Solid curve is simulated by using Eq. (1).

not exactly determined because of the uncertainty of the spot size of the laser beams at the interaction region. Therefore, we obtained only the relative absorption cross sections from the saturated DFWM signal intensities which are listed in Table I.

Figure 3(a) shows the LIF and Fig. 3(b) shows the DFWM spectra of the $\tilde{C}\leftarrow\tilde{X}$ transition of jet-cooled SO_2. The DFWM spectrum was measured under a condition of the high laser power limit, while the LIF spectrum was measured at low laser power condition to avoid saturation effect. The assignment of vibronic bands observed in the region below the dissociation threshold has been presented by several groups by the LIF spectrum[5,8,9] and the assignment is given in Fig. 3. In the LIF spectrum, two main progressions have been assigned to the series involving the bending vibration, that is, $(\nu_1,\nu_2,\nu_3)=(1,n,2)$ and $(3,n,0)$.[5,8,9] Above the dissociation threshold, the assignment of each vibronic band is

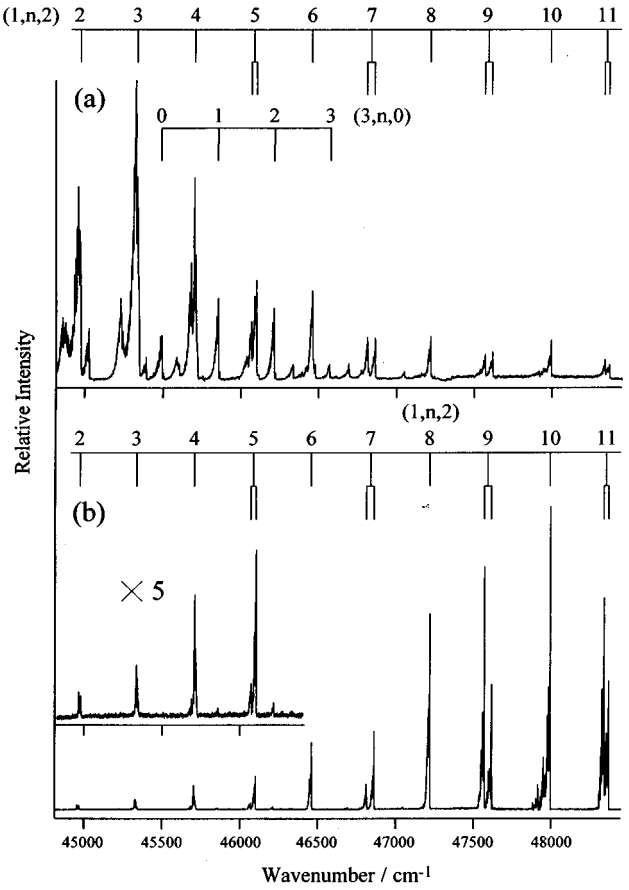

FIG. 3. (a) LIF and (b) DFWM spectra of the $\tilde{C}\ ^1B_2\leftarrow\tilde{X}\ ^1A_1$ transition of jet-cooled SO_2.

TABLE I. Energies, assignments (ν_1,ν_2,ν_3), relative DFWM intensity, fluorescence decay rate, relative fluorescence quantum yield (Φ), O atom production rate, and IC rate of the $\tilde{C}$ state of SO_2.

Energy/cm^{-1}	Assignment (ν_1,ν_2,ν_3)	Relative DFWM intensity[a]	Fluorescence decay rate /10^7 s^{-1}	Φ	Production rate /10^7 s^{-1}	k_{IC} /10^7 s^{-1}
44 966.8	(1,2,2)	1.7	2.5	1		
45 334.8	(1,3,2)	3.4	2.5	0.76		
45 707.1	(1,4,2)	8.1	17	0.21	14	6.5
46 101.9	(1,5,2)	11	14	0.076	13	23
46 460.8	(1,6,2)	22		0.034		53
46 812.7	(1,7,2)	8.5		0.041		44
46 863.2	(1,7,2)	26		0.013		140
47 220.6	(1,8,2)	65		0.0056		340
47 572.5	(1,9,2)	80		0.0026		730
47 620.1	(1,9,2)	41		0.0055		340
47 999.0	(1,10,2)	100		0.0033		570
48 347.6	(1,11,2)	70		0.0023		820
48 377.1	(1,11,2)	42		0.0027		700
45 496.9	(3,0,0)		2.6	0.74		1.8
45 856.8	(3,1,0)		4.3	0.44	4.8	3.4
46 213.8	(3,2,0)		5.9	0.32	5.6	4.0
46 570.0	(3,3,0)			0.29	6.7	

[a]The relative DFWM intensities are normalized so that the (1,10,2) band intensity is equal to 100.

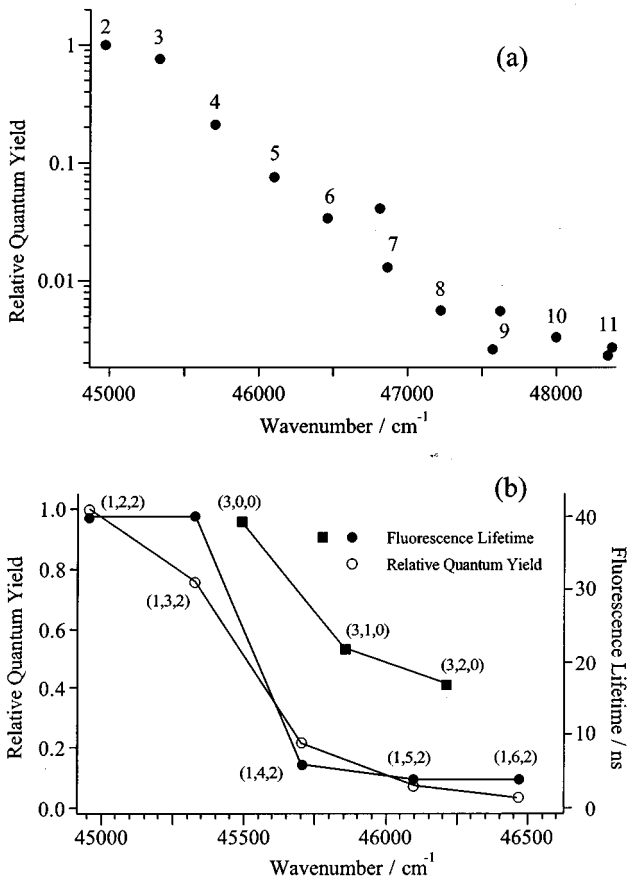

FIG. 4. (a) Relative fluorescence quantum yield (RFQY) of the $(1,n,2)$ series vs the excitation energy. (b) Energy dependence of the RFQY and the fluorescence lifetime in energy region from 45 000 cm^{-1} to 46 500 cm^{-1}.

not straightforward due to anharmonic coupling, i.e., Fermi resonance and/or Coriolis coupling.[8,12,34] From the result of the DFWM spectrum, however, we conclude that the bending progression of the $(1,n,2)$ series shows prominent feature toward the higher energy region across the dissociation threshold. It is also seen that the $(1,n,2)$ bands having odd ν_2 number are split in two bands in the figure.

The most remarkable difference between the DFWM and the LIF spectra is seen in the energy region higher than 45 700 cm^{-1}. In the DFWM spectrum the intensity of the $(1,n,2)$ progression increases with n, while the same series in the LIF spectrum suddenly drops at the (1,4,2) band. The decrease of the LIF intensity above the (1,4,2) band has been known to be due to the nonradiative process, that is, predissociation. Since the DFWM spectrum represents the absorption intensities of these series, we have obtained the relative fluorescence quantum yield (RFQY) by taking ratios of the band intensities of the LIF and the DFWM spectra. Figure 4(a) shows a logarithmic plot of the RFQY of the $(1,n,2)$ series vs energy. It is noticed that the logarithmic value of the RFQY decreases almost linearly with energy, which will be discussed later, and that RFQY in the higher energy region does not go to zero completely but stays constant with a small value. Another interesting point in Fig. 3 is that the $(3,n,0)$ series is very weak in the DFWM spectrum, whereas it is as intense as the $(1,n,2)$ series in the LIF spectrum. The difference is described by that the RFQY of the $(3,n,0)$ series is larger than that of the $(1,n,2)$ series, that is, the nonradiative rate of the $(1,n,2)$ series is larger than the $(3,n,0)$ series. This vibrational mode dependence was also reported by Vasudev *et al.*, who found that the fluorescence intensity after two-photon absorption depend on the pressure above the dissociation limit.[9] They suggested that the vibronic levels involving the ν_3 mode are more predissociative and the predissociation competes with the collisional relaxation.

For the $(3,n,0)$ series, we could not obtain the RFQY from the DFWM spectrum, because the absorption intensity of this series is too weak to measure the spectrum at high power limit. Instead of obtaining RFQY, we measured fluorescence lifetimes for this series in the energy region from 45 000 to 46 500 cm^{-1}. Figure 4(b) shows a plot of the observed fluorescence lifetimes of the $(3,n,0)$ and $(1,n,2)$ series, and also the RFQY for the $(1,n,2)$ series of the same region. As can be seen in Fig. 4(b), a good agreement is obtained in the vibrational mode dependence between the two measurements. The fluorescence lifetime of the $(3,n,0)$ level is roughly four times longer than the $(1,n,2)$ levels above the dissociation threshold. It is concluded that the bands involving ν_3 mode decay much faster than other vibronic bands and ν_3 modes is acting as a promoting mode for the nonradiative decay process which leads to the predissociation.

There are two important results obtained from the RFQY measurement.

(1) The logarithmic plot of RFQY for $(1,n,2)$ series decreases linearly with internal energy.

(2) The ν_3 mode acts as a promoting mode for the nonradiative (predissociation) process.

The characteristic vibrational mode dependence of RFQY can be explained by assuming that the nonradiative process proceeds through internal conversion (IC) to the $\tilde{X}$ state. The IC rate of the $\tilde{C}$ state could be explained by Fermi Golden Rule

$$k_{\tilde{X}\leftarrow\tilde{C}}=\frac{2\pi}{\hbar}\,|\langle\Psi_{\tilde{X}}|H'|\Psi_{\tilde{C}}\rangle|^2\rho(E), \tag{7}$$

where $H'=\partial^2/\partial Q^2$ is the perturbation Hamiltonian between $\tilde{C}$ and $\tilde{X}$, and $\rho(E)$ is the density of states of $\tilde{X}$ state. We assume that the zeroth-order vibronic states are described as usual in Born–Oppenheimer approximation

$$\Psi_{\tilde{X}}=\varphi_{\tilde{X}}(r,Q)\chi_{\tilde{X}}(Q), \quad \Psi_{\tilde{C}}=\varphi_{\tilde{C}}(r,Q)\chi_{\tilde{C}}(Q). \tag{8}$$

Here $\varphi_{\tilde{X}}$ and $\varphi_{\tilde{C}}$ are electronic wave functions, which depend on nuclear coordinates Q. $\chi_{\tilde{X}}$ and $\chi_{\tilde{C}}$ are vibrational wave functions. The matrix element of IC is expressed as

$$\langle\Psi_{\tilde{X}}|H'|\Psi_{\tilde{C}}\rangle\approx\sum_k v_{\mathrm{el}}^k\langle\chi_{\tilde{X}k}(Q_k)|\frac{\partial}{\partial Q_k}|\chi_{\tilde{C}k}(Q_k)\rangle \times\prod_{j\neq k}\langle\chi_{\tilde{X}j}(Q_j)|\chi_{\tilde{C}j}(Q_i)\rangle, \tag{9}$$

where

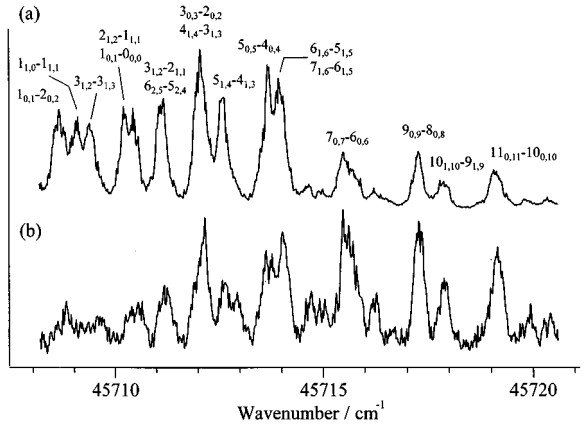

FIG. 5. Rotationally resolved (a) LIF and (b) DFWM spectra of the (1,4,2) band. The assignments of the rotational structure are based on Ref. 6.

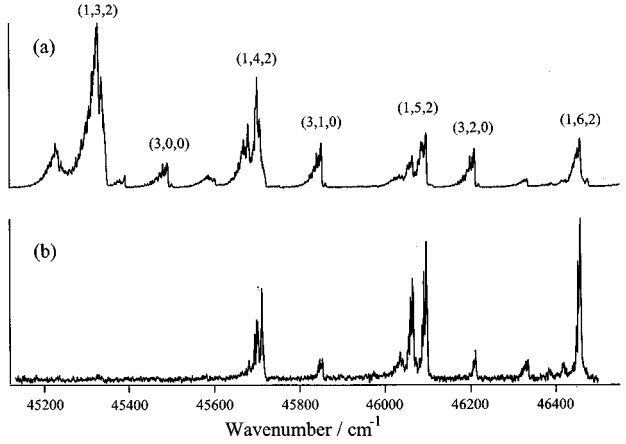

FIG. 6. (a) LIF and (b) photofragment yield spectra of the SO_2. Photofragment yield spectrum was obtained by monitoring the O atom fragment.

$$v_{\mathrm{el}}^{k}=-\frac{\hbar^2}{M_k}\frac{\langle\varphi_{\tilde{X}}(r,Q_0)|\{\partial U(r,Q)/\partial Q_k\}_0|\varphi_{\tilde{C}}(r,Q_0)\rangle}{E_{\tilde{X}}(0)-E_{\tilde{C}}(0)}. \tag{10}$$

Here $U(r,Q)$ is the Coulomb potential of the nuclear and electrons. By taking into account that the $\tilde{C}$ state belongs to B_2 and the $\tilde{X}$ state belongs to A_1 symmetric species, respectively, it is seen that the electronic part v_{el}^{k} has a nonvanishing value through the ν_3 (b_2) mode. The same mode can also act as a promoting mode for vibrational overlap integral in Eq. (9). The difference of IC rate between $(1,n,2)$ and $(3,n,0)$ series is considered as a difference of magnitude of vibrational overlap integral given by Eq. (9). As a result, we conclude that the initial step of the predissociation of SO_2 in the $\tilde{C}$ state is the internal conversion to the $\tilde{X}$ state.

As to the (1,4,2) band, Becker *et al.* showed that predissociation threshold lies near the $J'_{K'_P,K'_O}=6_{2,5}$ by comparison of LIF and photofragment yield spectra.[6,7] We also investigated the rotational dependence of the predissociation. Figure 5 shows the R-branch region of the rotationally resolved DFWM and LIF spectra of the (1,4,2) band. The assignments of the rotational structures are based on Ref. 6. It is clearly seen that the LIF signal intensity is weak at $J'\geqslant 7_{0,7}$ compared with the DFWM spectrum. Though we could not identified the occurrence of the predissociation at $J'=6_{2,5}$ due to the overlap with an other rotational line, we could confirm the levels with $J'\geqslant 7$ predissociate from the present experiment.

B. Photofragment yield spectrum

From the result of the DFWM spectrum and the fluorescence lifetime measurement, it is concluded that IC takes place as the initial nonradiative process prior to the dissociation. We then observed generation rates of O atom fragment to examine whether IC is the rate determining process for the dissociation.

We first measured the action spectrum by monitoring the O atom fragment with $(2+1)$ REMPI through the $3p\ ^3P_{J'}\leftarrow 2p\ ^3P_2$ transition. The delay-time between pump and probe laser pulses was set to 20 ns. Figure 6(a) shows the LIF and Fig. 6(b) shows the O atom yield spectra. It is clearly seen that dissociation occurs above the (1,4,2) band. From the O atom yield measurement and the RFQY measurement, it was confirmed that the band at which the nonradiative process occurs is the same band at which the dissociation occurs. We then measured the rise time of O atom production by changing the delay-time between the pump and probe lasers. Figure 7(a) shows the results for the (3,1,0) band and Fig. 7(b) shows the results for the (1,5,2) band.

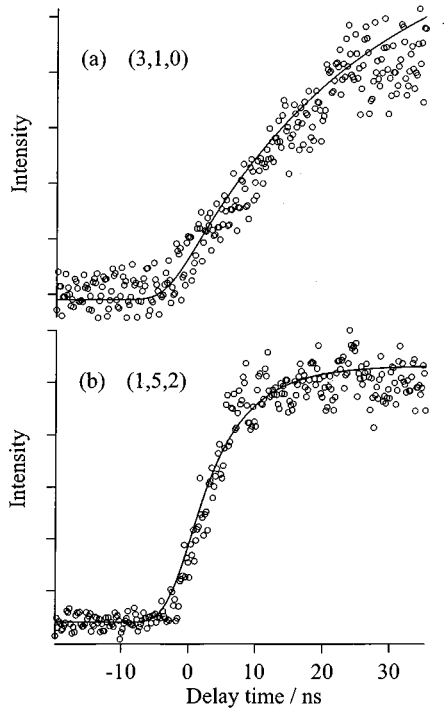

FIG. 7. The time profile of the O (^3P) generation as a function of delay time for (a) the (3,1,0) band and (b) the (1,5,2) band. The curve obtained from the least-squares fit is also shown. The O (^3P) atom generation rate of the (3,1,0) is $k=4.8\times10^7\ \mathrm{s}^{-1}$ and, for the (1,5,2) band, $k=1.3\times10^8\ \mathrm{s}^{-1}$. See text.

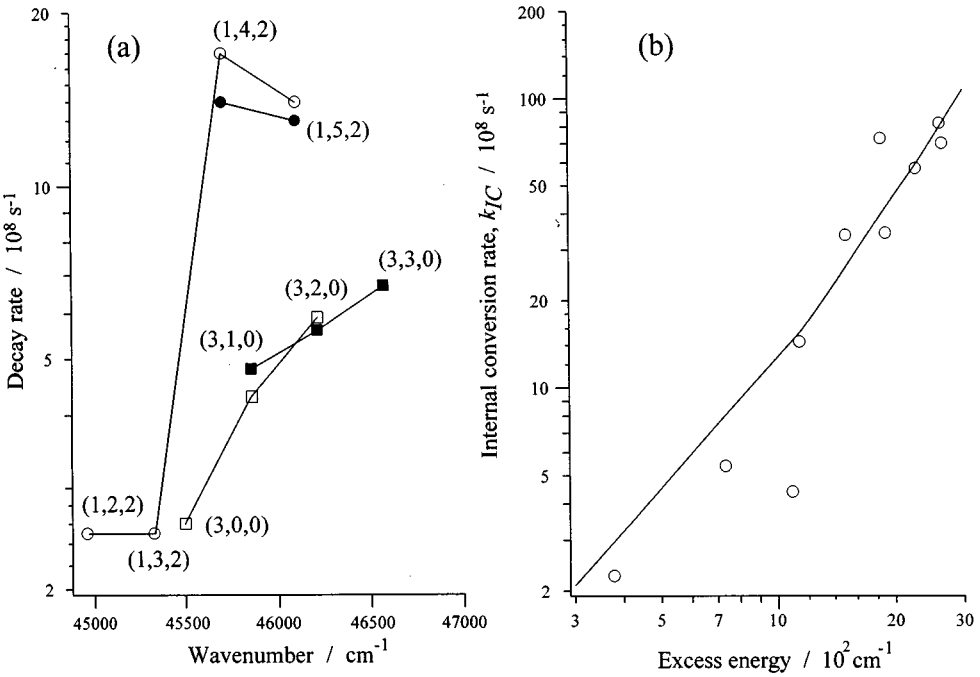

FIG. 8. (a) Logarithmic plot of the decay rate and the O atom production rate as function of the excitation energy. (○) and (□) refer to the decay rates of (1,*n*,2) and (3,*n*,0) series, respectively. (●) and (■) refer to the O atom production rates of (1,*n*,2) and (3,*n*,0) series, respectively. (b) Logarithmic plot of the internal conversion (IC) rate as function of the excess energy. The solid curve is the IC rate calculated by using Eqs. (6) and (13). See text.

Figure 7 also shows a fitted curve obtained by a least-square fit assuming that the time profile of the rise curve to be $A(1-e^{-kt})$. Here, we assumed triangular pulse shapes for the pump laser Nd:YAG laser pumped dye laser [FWHM (full width at half maximum)=5 ns] and for the probe laser excimer laser pumped dye laser (FWHM=10 ns). The production rates, k, are listed in Table I, and also plotted in Fig. 8(a). We also plotted the total decay rate of the $\tilde{C}$ state in Fig. 8(a). As can be seen in Fig. 8(a), the O atom production rate agrees very well with the total decay rate of the $\tilde{C}$ state with respect to not only the absolute value but also the vibrational dependence. Thus we can conclude that the dissociation occurs immediately after the IC to the $\tilde{X}$ state.

Finally, we obtained the IC rate of the $\tilde{C}$ state of SO_2 from the RFQY measurement and the fluorescence lifetime measurement. The IC rate, k_{IC}, is expressed by

$$k_{\mathrm{IC}}=(k_r+k_{nr})\left(\frac{\Phi_{(1,3,2)}-\Phi_{(1,n,2)}}{\Phi_{(1,n,2)}}\right). \tag{11}$$

Here, k_r is the radiative decay rate and k_{nr} is the nonradiative decay rate which does not include the IC rate. We assumed that k_{nr} is constant through all the vibronic bands. This may be a reasonable assumption because the reported fluorescence decay rates are almost the same for the vibronic bands below the dissociation threshold, that is k_{nr} is constant.[2] Thus, this behavior is assumed to be the same even above the threshold, since the nonradiative process is thought to occur independent of the internal conversion. The obtained results are plotted in Fig. 8(b) for the (1,*n*,2) series. As can be seen in Fig. 8(b), the logarithmic plot of the IC rate of the (1,*n*,2) series shows a linear dependence vs excess energy. We examined the observed energy dependence of k_{IC} in terms of phase space theory (PST). Since the vibrational quantum number of the promoting mode, ν_3, is the same through the (1,*n*,2) series, the matrix element in Eq. (6) is assumed to be the same. So we evaluated $\rho(E)$ to investigate the excess energy dependence of the IC rate. The density of state, $\rho(E)$, is expressed by the product of $\rho(E_t)$: density of states of relative translation between SO and O fragments, $\rho(E_{\mathrm{SO}})$: density of states of the internal mode of SO, and $\rho(E_{\mathrm{O}})$: degeneracy of spin–orbit sublevels of O (^3P_J). The energy conservation implies that

$$E^{\dagger}=E_{\mathrm{SO}}(v,J_{\mathrm{SO}})+E_{\mathrm{O}}(J_{\mathrm{O}})+E_t. \tag{12}$$

E_{SO} and E_{O} are the internal energies of the fragments SO and O, respectively, and $E^{\dagger}$ is the excess energy above the dissociation threshold, D_0. $\rho(E_t)$ is given by $\rho(E_t)\propto E_t^{1/2}$. For $\rho(E_{\mathrm{SO}})$ we consider the degeneracy of molecular rotation. The total density of state at a given $E^{\dagger}$ is expressed by

$$\rho(E^{\dagger})=A_t\sum_{J_{\mathrm{O}}=0}^{2}\sum_{v=0}^{v^{\max}}\sum_{J_{\mathrm{SO}}=0}^{J^{\max}}(2J_{\mathrm{O}}+1)(2J_{\mathrm{SO}}+1)\times[E^{\dagger}-E_{\mathrm{SO}}(v,J_{\mathrm{SO}})-E_{\mathrm{O}}(J_{\mathrm{O}})]^{1/2}, \tag{13}$$

where A_t is a proportionality constant. For the density of states of the J level of the O (^3P_J), Becker *et al.*[7] reported that $J=2$ is the dominant product, and Eq. (13) is simplified as follows:

$$\rho(E^{\dagger}) = 5A_t \sum_{v=0}^{v^{\max}} \sum_{J_{SO}=0}^{J^{\max}} (2J_{SO}+1) \times \{E^{\dagger} - E_v - [BJ_{SO}(J_{SO}+1)]\}^{1/2} = \frac{10A_t}{3B} \sum_{v=0}^{v^{\max}} (E^{\dagger} - E_v)^{3/2}, \quad (14)$$

where B refers to a rotational constant of SO molecule. Figure 8(b) shows a logarithmic plot of Eq. (13) vs its available energy, where we used the dissociation energy of $D_0 = 45\,725.3\ \mathrm{cm}^{-1}$ reported by Becker *et al.*[7] As can be seen in the figure, the calculated dependence of the IC rate on the excess energy by use of Eqs. (6) and (13) is in good agreement with that of the IC rate obtained from the RFQY measurement and the increase of k_{IC} is explained to be due to the increase of the density of states. Becker *et al.* also applied the phase space theory to simulate the rotational distributions of the SO fragment and reported that the simulated distribution is in good agreement with the observed one.

In conclusion, we applied DFWM spectroscopy to the $\tilde{C}\ ^1B_2 \leftarrow \tilde{X}\ ^1A_1$ transition of jet-cooled SO_2 molecules. By comparing the DFWM spectrum with the LIF spectrum, the relative fluorescence quantum yield for the $\tilde{C}$ state of SO_2 was obtained under an isolated molecule condition. It was found that the predissociation rate depends not only on the excess energy but also on the vibrational mode. The occurrence of the predissociation above the (1,4,2) level was confirmed by the O (^3P) atom detection. It was also found that the generation rate of O atom coincides with the fluorescence decay rate. As the result, it is concluded that the predissociation mainly occurs through the internal conversion to the $\tilde{X}$ state and the internal conversion is the rate determining process for the dissociation.

[1] H. Okabe, J. Am. Chem. Soc. **93**, 7095 (1971).
[2] M. H. Hui and S. A. Rice, Chem. Phys. Lett. **17**, 474 (1972).
[3] M. Ivanco, J. Hager, W. Sharfin, and S. C. Wallace, J. Chem. Phys. **78**, 6531 (1983).
[4] H. Kanamori, J. E. Bulter, K. Kawaguchi, C. Yamada, and E. Hirota, J. Chem. Phys. **83**, 611 (1985).
[5] T. Ebata, O. Nakazawa, and M. Ito, Chem. Phys. Lett. **143**, 31 (1988).
[6] S. Becker, C. Braatz, J. Lindner, and E. Tiemann, Chem. Phys. Lett. **208**, 15 (1993).
[7] S. Becker, C. Braatz, J. Lindner, and E. Tiemann, Chem. Phys. **196**, 275 (1995).
[8] K. Yamanouchi, M. Okunishi, Y. Endo, and S. Tsuchiya, J. Mol. Struct. **352/353**, 541 (1995).
[9] R. Vasudev and W. M. McClain, J. Mol. Spectrosc. **89**, 125 (1981).
[10] C. S. Effenhauser, P. Felder, and J. R. Huber, Chem. Phys. **142**, 311 (1990).
[11] A. Freedman, S. C. Yang, and R. Bersohn, J. Chem. Phys. **70**, 5313 (1979).
[12] J. C. D. Brand, P. H. Chiu, A. R. Hoy, and H. D. Bist, J. Mol. Spectrosc. **60**, 43 (1976).
[13] M. Kawasaki and H. Sato, Chem. Phys. Lett. **139**, 585 (1987).
[14] P. Felder, C. S. Effenhauser, B. M. Haas, and J. R. Huber, Chem. Phys. Lett. **148**, 417 (1988).
[15] T. J. Butenhoff and E. A. Rohlfing, J. Chem. Phys. **98**, 5460 (1993).
[16] T. J. Butenhoff and E. A. Rohlfing, J. Chem. Phys. **98**, 5469 (1993).
[17] R. Farrow, D. J. Rakestraw, and T. Dreier, J. Opt. Soc. Am. B **9**, 1770 (1992).
[18] R. L. Abrams and R. C. Lind, Opt. Lett. **2**, 94 (1978).
[19] R. L. Abrams and R. C. Lind, Opt. Lett. **3**, 205 (1978).
[20] S. Williams, R. N. Zare, and L. R. Rahn, J. Chem. Phys. **101**, 1072 (1994).
[21] S. Williams, R. N. Zare, and L. R. Rahn, J. Chem. Phys. **101**, 1093 (1994).
[22] S. Williams, L. R. Rahn, and R. N. Zare, J. Chem. Phys. **104**, 3947 (1996).
[23] G. Alber, J. Cooper, and P. Ewart, Phys. Rev. A **31**, 2344 (1985).
[24] J. Cooper, A. Charlton, D. R. Meacher, P. Ewart, and G. Alber, Phys. Rev. A **40**, 5705 (1989).
[25] D. R. Meacher, A. Charlton, P. Ewart, J. Cooper, and G. Alber, Phys. Rev. A **42**, 3018 (1990).
[26] Y. Tang and S. A. Reid, J. Chem. Phys. **105**, 8481 (1996).
[27] R. P. Lucht, R. L. Farrow, and D. J. Rakestraw, J. Opt. Soc. Am. B **10**, 1508 (1993).
[28] J. F. Lam and R. L. Abrams, Phys. Rev. A **26**, 1539 (1982).
[29] P. R. Berman, D. G. Steel, G. Khitrova, and J. Liu, Phys. Rev. A **38**, 252 (1988).
[30] R. L. Abrams, J. F. Lam, R. C. Lind, D. G. Steel, and P. L. Liao, in *Optical Phase Conjugation, Quantum Electronics—Principles and Applications*, edited by R. A. Fisher (Academic, New York, 1983), Chap. 8.
[31] P. H. Vaccaro, in *Molecular Dynamics and Spectroscopy by Stimulated Emission Pumping*, Vol. 4 of *Advanced Series in Physical Chemistry*, edited by H. L. Dai and R. W. Field (World Scientific, London, 1995), Chap. 1.
[32] R. W. Boyd, *Nonlinear Optics* (Academic, New York, 1992).
[33] S. Williams, D. S. Green, S. Sethuraman, and R. N. Zare, J. Am. Chem. Soc. **114**, 9122 (1992).
[34] A. R. Hoy and J. C. D. Brand, Mol. Phys. **36**, 1409 (1978).